Schmidt-Kalman Filter with Polynomial Chaos Expansion for Orbit Determination of Space Objects

Yang Yang, Han Cai, Kefei Zhang
SPACE Research Centre, RMIT University, VIC 3001, Australia

ABSTRACT

Parameter errors in orbital models can result in poor orbit determination (OD) using a traditional Kalman filter. One approach to account for these errors is to consider them in the so-called Schmidt-Kalman filter (SKF), by augmenting the state covariance matrix (CM) with additional parameter covariance rather than additively estimating these so-called "consider" parameters. This paper introduces a new SKF algorithm with polynomial chaos expansion (PCE-SKF). The PCE approach has been proved to be more efficient than Monte Carlo method for propagating the input uncertainties onto the system response without experiencing any constraints of linear dynamics, or Gaussian distributions of the uncertainty sources. The state and covariance needed in the orbit prediction step are propagated using PCE. An inclined geosynchronous orbit scenario is set up to test the proposed PCE-SKF based OD algorithm. The satellite orbit is propagated based on numerical integration, with the uncertain coefficient of solar radiation pressure considered. The PCE-SKF solutions are compared with extended Kalman filter (EKF), SKF and PCE-EKF (EKF with PCE) solutions. It is implied that the covariance propagation using PCE leads to more precise OD solutions in comparison with those based on linear propagation of covariance.

1. INTRODUCTION

Due to the rapid increase in the population of earth-orbiting objects, state estimation of these space objects for mission planning and collision avoidance is therefore of great significance. The Kalman filtering technique is widely used for orbit determination (OD), which combines both orbit prediction (OP) and observation update together in a sequential manner. However, non-gravitational perturbations, e.g. solar radiation pressure and atmosphere drag acting on the space objects, cannot be modelled precisely in the OP process due to the uncertainties associated with these parameters. This leads to deteriorated OD results using the traditional Kalman filter.

One approach to account for parameter errors in a dynamic system is to consider them in the so-called Schmidt-Kalman filter (SKF), by augmenting the state covariance matrix (CM) with additional parameter CM rather than additively estimating these so-called "consider" parameters. This methodology originated by S. F. Schmidt in the mid 1960s [1] is especially useful when parameters have low observability [2]. Zanetti et al. [3] addressed the issues with relation to recursive implementation of SKF. Stauch and Jah incorporated the SKF into an unscented Kalman filter framework [4]. A SKF based orbit determination scheme is introduced in [5] with a simplified orbit dynamical model for onboard computing, where the atmospheric drag and solar radiation pressure coefficients are considered.

In order to obtain optimal estimates, filters need to handle uncertainties involved in the system's dynamics and associated observations. As an alternative to statistical methods, the polynomial chaos expansions (PCE) method is proposed to account for the effects of arbitrary, time-invariant uncertainties associated with model parameters and initial conditions [6]. The PCE approach has been proved to be more efficient than Monte Carlo method for propagating the input uncertainties onto the system response, by establishing an alternative deterministic surrogate system with linear combination of orthogonal basis functions. Any constraints of linear dynamics, or Gaussian distributions of the uncertainty sources are no longer required in PCE. It has been integrated with filters for state and parameter estimation [7–9].

This paper introduces a new SKF algorithm with polynomial chaos expansion (PCE-SKF) for orbit determination. The state and covariance needed in the OP step are propagated using PCE. More specifically, the CM is computed from samples generated in PCE instead of linear propagation by the state transition matrix (STM) and sensitivity matrix (SM). The proposed PCE-SKF is applied to OD of space objects. An inclined geosynchronous orbit (IGSO)

scenario is set up to test the proposed algorithm. The satellite orbit is propagated based on numerical integration, with the uncertain solar radiation pressure (SRP) coefficient considered. Range observations from three ground stations are used in the measurement update step. To evaluate the impact of SRP coefficient into the OD accuracy, both Gaussian and uniform distributions are used to represent the uncertainty associated with the SRP coefficient. The PCE-SKF solutions are compared with those using extended Kalman filter (EKF), SKF and PCE-EKF (EKF with PCE).

The rest of the paper is organised as follows. Section 2 revisits the Schmidt-Kalman filter for state estimation and parameter compensation. The polynomial chaos expansion approach for uncertainty propagation is introduced in Section 3, followed by a description of the proposed PCE-SKF algorithm for orbit determination. After this, a numerical example is given to test the PCE-SKF algorithm and conclusions are presented.

2. SCHMIDT-KALMAN FILTER

We formulate the nonlinear orbit dynamics and the measurement equation into a discrete form in order to be implemented in the SKF:

$$\boldsymbol{X}_k = g(\boldsymbol{X}_{k-1}, \boldsymbol{w}_k), \tag{1a}$$

$$\boldsymbol{y}_k = h(\boldsymbol{X}_k, \boldsymbol{v}_k), \tag{1b}$$

where the augmented state $\boldsymbol{X}$ is composed of both the orbital state $\boldsymbol{x}$ and "consider" parameters $\boldsymbol{p}$, and the subscript k indicates the time index. The operator $\boldsymbol{g}$ represents the numerical integration operator for the orbit propagation. But the "consider" parameters $\boldsymbol{p}$ are kept constants all the time. $\boldsymbol{h}$ denotes the nonlinear measurement function. $\boldsymbol{w}$ and $\boldsymbol{v}$ indicate the process noise and measurement noise, respectively, both of which are assumed to be white noise sources. Specifically, these distributions are given by:

$$\begin{aligned} \boldsymbol{w}_k &\sim \mathcal{N}(\boldsymbol{0}, \boldsymbol{Q}_k), \\ \boldsymbol{v}_k &\sim \mathcal{N}(\boldsymbol{0}, \boldsymbol{R}_k). \end{aligned} \tag{2}$$

In the prediction step of the SKF, satellite trajectory is propagated using Eq. 3, while the "consider" parameter vector $\boldsymbol{p}$ is kept constant in Eq. 4:

$$\hat{\boldsymbol{x}}_k^- = \boldsymbol{f}(\hat{\boldsymbol{x}}_{k-1}^+, \hat{\boldsymbol{p}}_{k-1}^+, \boldsymbol{0}), \tag{3}$$

$$\hat{\boldsymbol{p}}_k^- = \hat{\boldsymbol{p}}_{k-1}^+. \tag{4}$$

On the other hand, the covariance matrix $\boldsymbol{P}$ is predicted for each block as shown in Eq. 5:

$$\begin{bmatrix} \hat{\boldsymbol{P}}_x & \hat{\boldsymbol{P}}_{xp} \\ \hat{\boldsymbol{P}}_{px} & \hat{\boldsymbol{P}}_p \end{bmatrix}_k^- = \begin{bmatrix} \hat{\boldsymbol{\Theta}} & \hat{\boldsymbol{\Psi}} \\ \boldsymbol{0} & \boldsymbol{I} \end{bmatrix}_{k-1} \begin{bmatrix} \hat{\boldsymbol{P}}_x & \hat{\boldsymbol{P}}_{xp} \\ \hat{\boldsymbol{P}}_{px} & \hat{\boldsymbol{P}}_p \end{bmatrix}_{k-1}^+ \begin{bmatrix} \hat{\boldsymbol{\Theta}}^T & \boldsymbol{0} \\ \hat{\boldsymbol{\Psi}}^T & \boldsymbol{I} \end{bmatrix}_{k-1} + \begin{bmatrix} \boldsymbol{Q}_x & \boldsymbol{0} \\ \boldsymbol{0} & \boldsymbol{Q}_p \end{bmatrix}_{k-1}, \tag{5}$$

where $\boldsymbol{\Theta}$ and $\boldsymbol{\Psi}$ denote the STM and sensitivity matrix, respectively. Solutions of these matrices can be found in Ref. [10].

By expanding Eq. 5, one can obtain the formulas for predictions of each block, as shown in Eq. 6-9:

$$\begin{aligned} \hat{\boldsymbol{P}}_{x,k}^- &= (\boldsymbol{\Theta}_{k-1}\hat{\boldsymbol{P}}_{x,k-1}^+ + \boldsymbol{\Psi}_{k-1}\hat{\boldsymbol{P}}_{px,k-1}^+)\boldsymbol{\Theta}_{k-1}^T \\ &+ (\boldsymbol{\Theta}_{k-1}\hat{\boldsymbol{P}}_{xp,k-1}^+ + \boldsymbol{\Psi}_{k-1}\hat{\boldsymbol{P}}_{p,k-1}^+)\boldsymbol{\Psi}_{k-1}^T + \boldsymbol{Q}_{x,k-1}, \end{aligned} \tag{6}$$

$$\hat{\boldsymbol{P}}_{xp,k}^- = \boldsymbol{\Theta}_{k-1}\hat{\boldsymbol{P}}_{xp,k-1}^+ + \boldsymbol{\Psi}_{x,k-1}\hat{\boldsymbol{P}}_{p,k-1}^+, \tag{7}$$

$$\hat{\boldsymbol{P}}_{px,k}^- = \hat{\boldsymbol{P}}_{px,k-1}^+\boldsymbol{\Theta}_{k-1}^T + \hat{\boldsymbol{P}}_{p,k-1}^+\boldsymbol{\Psi}_{k-1}^T = \hat{\boldsymbol{P}}_{xp,k}^{-,T}, \tag{8}$$

$$\hat{\boldsymbol{P}}_{p,k}^- = \hat{\boldsymbol{P}}_{p,k-1}^+ + \boldsymbol{Q}_{p,k-1}. \tag{9}$$

The update step of the SKF reads,

$$\begin{bmatrix}\hat{\boldsymbol{x}}\\ \hat{\boldsymbol{p}}\end{bmatrix}_k^+ = \begin{bmatrix}\hat{\boldsymbol{x}}\\ \hat{\boldsymbol{p}}\end{bmatrix}_k^- + \begin{bmatrix}\boldsymbol{K}_x(\boldsymbol{y}-\boldsymbol{h}(\hat{\boldsymbol{x}},\boldsymbol{0}))\\ \boldsymbol{0}\end{bmatrix}_k^-, \tag{10}$$

$$\begin{aligned}\begin{bmatrix}\hat{\boldsymbol{P}}_x & \hat{\boldsymbol{P}}_{xp}\\ \sim & \hat{\boldsymbol{P}}_p\end{bmatrix}_k^+ &= \left\{\begin{bmatrix}\boldsymbol{I} & 0\\ 0 & \boldsymbol{I}\end{bmatrix} - \begin{bmatrix}\boldsymbol{K}_x\\ \boldsymbol{0}\end{bmatrix}_k \begin{bmatrix}\boldsymbol{H}_x & \boldsymbol{0}\end{bmatrix}_k\right\} \times \begin{bmatrix}\hat{\boldsymbol{P}}_x & \hat{\boldsymbol{P}}_{xp}\\ \sim & \hat{\boldsymbol{P}}_p\end{bmatrix}_k^-\\ &\times \left\{\begin{bmatrix}\boldsymbol{I} & 0\\ 0 & \boldsymbol{I}\end{bmatrix} - \begin{bmatrix}\boldsymbol{K}_x\\ \boldsymbol{0}\end{bmatrix}_k \begin{bmatrix}\boldsymbol{H}_x & \boldsymbol{0}\end{bmatrix}_k\right\}^T + \begin{bmatrix}\boldsymbol{K}_x\\ \boldsymbol{0}\end{bmatrix}_k \boldsymbol{R}_k \begin{bmatrix}\boldsymbol{K}_x & \boldsymbol{0}\end{bmatrix}_k^T,\end{aligned} \tag{11}$$

$$\boldsymbol{K}_{x,k} = \hat{\boldsymbol{P}}_{x,k}^- \hat{\boldsymbol{H}}_{x,k}^T (\hat{\boldsymbol{H}}_{x,k}\hat{\boldsymbol{P}}_{x,k}^- \hat{\boldsymbol{H}}_{x,k}^T + \boldsymbol{R}_k)^{-1}. \tag{12}$$

Expand Eq. 11 for each entry to obtain the following updating equations:

$$\hat{\boldsymbol{P}}_{x,k}^+ = (\boldsymbol{I}-\boldsymbol{K}_{x,k}\boldsymbol{H}_{x,k})\hat{\boldsymbol{P}}_{x,k}^- + \boldsymbol{K}_{x,k}\boldsymbol{R}_k\boldsymbol{K}_{x,k}^T, \tag{13}$$

$$\hat{\boldsymbol{P}}_{xp,k}^+ = (\boldsymbol{I}-\boldsymbol{K}_{x,k}\boldsymbol{H}_{x,k})\hat{\boldsymbol{P}}_{xp,k}^-, \tag{14}$$

$$\hat{\boldsymbol{P}}_{px,k}^+ = \hat{\boldsymbol{P}}_{xp,k}^{+,T}, \tag{15}$$

$$\hat{\boldsymbol{P}}_{p,k}^+ = \hat{\boldsymbol{P}}_{p,k}^-. \tag{16}$$

Note that the updating of the entry $\hat{\boldsymbol{P}}_{px,k}$ presented in Eq. 15 is not displayed in Eq. 11.

3. THE POLYNOMIAL CHAOS APPROACH

The polynomial chaos approach was firstly introduced by Norbert Wiener when Hermite polynomials were used to model stochastic processes with Gaussian random variables [11]. After Xiu extended the PCE to more general orthogonal polynomials using Wiener-Askey scheme [6], the PCE approach has recently regained its popularity for quantifying the propagation of uncertainty in nonlinear dynamical systems. The PCE framework has many attractive features which are potentially well suited for numerical computations with usually a substantially smaller computational effort compared to Monte Carlo sampling.

Generally two steps are involved in PCE algorithms: 1) the construction of a computationally efficient surrogate model of the system using the orthogonal polynomials and 2) the stochastic propagation of the initial uncertainties through evaluation of the surrogate model. In the context of PCE, the solution $\boldsymbol{X}$ of Eq. 1a can be represented by an infinite series of orthogonal polynomials [12]:

$$\begin{aligned}\boldsymbol{X}(t,\boldsymbol{\xi}) &= c_0\phi_0 + \sum_{i_1=1}^{d} c_{i_1}\phi_1(\xi_{i_1}) + \sum_{i_1=1}^{d}\sum_{i_2=1}^{i_1} c_{i_1 i_2}\phi_2(\xi_{i_1},\xi_{i_2})\\ &+ \sum_{i_1=1}^{d}\sum_{i_2=1}^{i_1}\sum_{i_3=1}^{i_2} c_{i_1 i_2 i_3}\phi_3(\xi_{i_1},\xi_{i_2},\xi_{i_3}) + \cdots\end{aligned} \tag{17}$$

where ϕ_k is the generalised polynomial basis function of order k determined using the Wiener-Askey scheme [6] based on the PDF of multidimensional random variables $\xi_{i_j}(i_j = 1,2,\ldots,d)$ that typically represent the uncertainties in model parameters or initial and boundary conditions. In the PCE context, the polynomial bases have been expanded into other types of functions. For instance, Legendre, Laguerre, and Jacobi are optimal selections for modelling the effects of random variable described by uniform, γ and β, respectively, in order to achieve theoretical exponential convergence of the approximation. The above expansions can be formulated into a concrete form via multidimensional basis functions, i.e.:

$$\boldsymbol{X}(t,\boldsymbol{\xi}) = \sum_{\boldsymbol{\alpha}\in\mathbb{N}_0^d} C_{\boldsymbol{\alpha}}\Phi_{\boldsymbol{\alpha}}(\boldsymbol{\xi}) \quad \left(\mathbb{N}_0^d := \{(\alpha_1,\ldots,\alpha_d) : \alpha_j \in \mathbb{N}\cup\{0\}\}\right) \tag{18}$$

where $\boldsymbol{\alpha}\in\mathbb{N}_0^d$ is a multidimentional index notation; $\Phi_k(\boldsymbol{\xi})$ denotes the multivariate basis function which is defined as the tensor product of univariate polynomial basis functions with the assumption that the random univariate variables

ξ_i are independent, identically distributed:

$$\Phi_{\boldsymbol{\alpha}}(\boldsymbol{\xi}) = \Phi_{\boldsymbol{\alpha}}(\xi_1, \xi_2, \ldots, \xi_d) = \phi^{(1)}_{\alpha_1}(\xi_1)\phi^{(2)}_{\alpha_2}(\xi_2)\cdots\phi^{(d)}_{\alpha_d}(\xi_d) \tag{19}$$

where $\alpha_d \in \mathbb{N}^1_0$ denotes the degree of the univariate polynomials $\phi^{(d)}_{\alpha_d}(\xi_d)$. In practice, the assemble of orthogonal polynomials in Eq. 18 needs to be truncated to a finite number. A standard truncation strategy corresponds to the total degree p of the polynomials and the dimensionality d of the random variables characterising the input uncertainties, hence the approximation of $\boldsymbol{X}$ with truncated PCE expansions is given as:

$$\hat{\boldsymbol{X}}(t, \boldsymbol{\xi}) = \sum_{\boldsymbol{\alpha}\in A^d_p} C_{\boldsymbol{\alpha}}\Phi_{\boldsymbol{\alpha}}(\boldsymbol{\xi}) \quad \left(A^d_p = \boldsymbol{\alpha} \in \mathbb{N}^d_0 : \|\boldsymbol{\alpha}\|_0 \leq d, \|\boldsymbol{\alpha}\|_1 \leq p\right). \tag{20}$$

3.1. ISOPROBABILISTIC TRANSFORMATION

In a real world scenario, the input variables for the system are always non-standard. In the context of gPC, isoprobabilistic transformations are introduced to transform the dependent random vector $\boldsymbol{X}$ into a Gaussian or a uniform vector [13]. Generally two steps are included: independency transformation (e.g. Nataf transformation [14, 15] with the Gaussian copula) and standardisation process.

According to Sklar's theorem, if the random variables have a joint distribution $F_{\boldsymbol{\xi}}(\boldsymbol{\xi})$ with n marginal distributions $F_1(\xi_1), \ldots, F_n(\xi_n)$, then there exists an n-dimensional copula C satisfying [13, 16]:

$$F_{\boldsymbol{\xi}}(\boldsymbol{\xi}) = C(F_1(\xi_1), \ldots, F_n(\xi_n)). \tag{21}$$

The Nataf transformation $T_1 : \mathbb{R}^n \to \mathbb{R}^n$ is used to get an independent Gaussian random vector [17]:

$$\bar{\boldsymbol{\xi}} = T_1(\boldsymbol{\xi}) = (\mathcal{N}^{-1}(\xi_1), \ldots, \mathcal{N}^{-1}(\xi_n)) \tag{22}$$

where $\mathcal{N}$ is a Gaussian distribution function and $\bar{\boldsymbol{\xi}}$ is a multivariate Gaussian random vector with standard random marginals. This transformation is feasible with known marginal distributions of $\boldsymbol{X}$ and the correlation matrix, which corresponds with the copula theory as well.

Then the transformation $T_2 : \mathbb{R}^n \to \mathbb{R}^n$ is used to obtain a standard Gaussian independent random vector $\boldsymbol{\eta}$:

$$\boldsymbol{\eta} = T_2(\bar{\boldsymbol{\xi}}). \tag{23}$$

For instance, in the case of Gaussian variables $\left\{\bar{\xi}_i \sim \mathcal{N}(\mu_i, \sigma_i)\right\}^d_{i=1}$, the transformation is expressed as:

$$\bar{\xi}_i = \mu_i + \sigma_i U_i, U_i \sim \mathcal{N}(0, 1). \tag{24}$$

Hence, the transformation

$$\boldsymbol{\eta} = T_{Gauss}(\boldsymbol{\xi}) = T_2(T_1(\boldsymbol{\xi})) \tag{25}$$

can be used to obtain the standard independent Gaussian random vector $\boldsymbol{\eta}$ from the dependent random vector $\boldsymbol{\xi}$.

With the isoprobabilistic transformation above, the approximate state $\boldsymbol{X}$ in Eq. 20 can be formulated as PCE with respect to the independent Gaussian vector $\boldsymbol{\eta}$:

$$\boldsymbol{X}(t, \boldsymbol{\eta}) = \sum_{\boldsymbol{\alpha}\in\mathbb{N}^d_0} C_{\boldsymbol{\alpha}}\Phi_{\boldsymbol{\alpha}}(T^{-1}_{Gauss}(\boldsymbol{\eta})) = \sum_{\boldsymbol{\alpha}\in\mathbb{N}^d_0} \bar{C}_{\boldsymbol{\alpha}}\Phi_{\boldsymbol{\alpha}}(\boldsymbol{\eta}). \tag{26}$$

3.2. NON-INTRUSIVE APPROACH TO SOLVE PCE COEFFICIENTS

To build up the approximation of the solution $\hat{\boldsymbol{X}}$ of Eq. 26, the polynomial coefficients need to be solved. The approaches can be categorised into two types: intrusive and non-intrusive approaches. In an intrusive approach, all the dependent random variables in the system equations are replaced with PCE expansions, which is straightforward but difficult to implement due to the fact of rewriting the whole program. Therefore, only non-intrusive approach is used in this work.

The system model is treated as a "black-box" so that the PCE coefficients are solved based on a set of simulation response evaluations. Generally two primary strategies have been proposed to calculate the polynomial coefficients

non-intrusively in the literature, i.e., the spectral projection and the least-squares regression (LSR) [14, 18]. The spectral projection method, like the common tensor-product quadrature strategy, generally suffers the curse of dimensionality. The LSR method is used in this work, which solves the coefficients $\boldsymbol{C}$ by minimising the cost function [14]:

$$\boldsymbol{C} \approx \arg\min_{\bar{C}_{\boldsymbol{\alpha}}} \frac{1}{M} \sum_{j=1}^{M} \left(\boldsymbol{X}(t, \boldsymbol{\eta}_j) - \sum_{\boldsymbol{\alpha} \in A_p^d} \bar{C}_{\boldsymbol{\alpha}} \Phi_{\boldsymbol{\alpha}}(\boldsymbol{\eta}_j) \right)^2 . \tag{27}$$

According to Eq. 27, the PCE expansions and corresponding coefficients can be written into a linear system:

$$\begin{bmatrix} \Phi_{\boldsymbol{\alpha}_1}(\boldsymbol{\eta}_1) & \Phi_{\boldsymbol{\alpha}_2}(\boldsymbol{\eta}_1) & \cdots & \Phi_{\boldsymbol{\alpha}_N}(\boldsymbol{\eta}_1) \\ \Phi_{\boldsymbol{\alpha}_1}(\boldsymbol{\eta}_2) & \Phi_{\boldsymbol{\alpha}_2}(\boldsymbol{\eta}_2) & \cdots & \Phi_{\boldsymbol{\alpha}_N}(\boldsymbol{\eta}_2) \\ \vdots & \vdots & \ddots & \vdots \\ \Phi_{\boldsymbol{\alpha}_1}(\boldsymbol{\eta}_M) & \Phi_{\boldsymbol{\alpha}_2}(\boldsymbol{\eta}_M) & \cdots & \Phi_{\boldsymbol{\alpha}_N}(\boldsymbol{\eta}_M) \end{bmatrix} \begin{bmatrix} \hat{\bar{C}}^T_{\boldsymbol{\alpha}_1} \\ \hat{\bar{C}}^T_{\boldsymbol{\alpha}_2} \\ \vdots \\ \hat{\bar{C}}^T_{\boldsymbol{\alpha}_N} \end{bmatrix} = \begin{bmatrix} \boldsymbol{X}^T(t, \boldsymbol{\eta}_1) \\ \boldsymbol{X}^T(t, \boldsymbol{\eta}_2) \\ \vdots \\ \boldsymbol{X}^T(t, \boldsymbol{\eta}_M) \end{bmatrix} . \tag{28}$$

The Eq. 28 can be formulated in a simple form:

$$\boldsymbol{H}\hat{\boldsymbol{C}} = \boldsymbol{Y} \tag{29}$$

where $\boldsymbol{H}$ is a $M \times N$ matrix, $\hat{\boldsymbol{C}}$ is the matrix of PCE coefficients, and $\boldsymbol{Y}$ is comprised of the surface response of the system model. The solution of the PCE coefficients can be given:

$$\hat{\boldsymbol{C}} = (\boldsymbol{H}^{\boldsymbol{T}}\boldsymbol{H})^{-\boldsymbol{1}}\boldsymbol{H}^{\boldsymbol{T}}\boldsymbol{Y}. \tag{30}$$

Figure 1 illustrates the degree of the N^{th} multivariate polynomial functions with respect to each univariate polynomial function. In this case, six inputs of position and velocity components are propagated using maximum 4^{th} degree PCE. The value of each coefficient is shown in Figure 2.

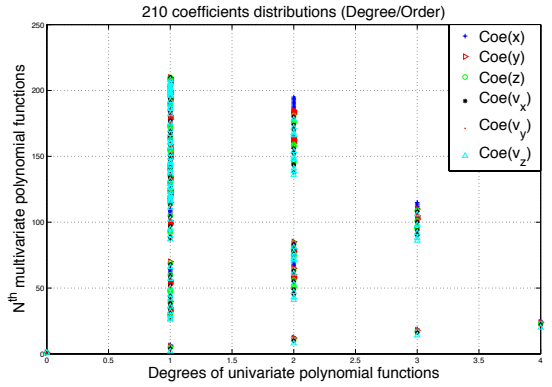

Fig. 1. Coefficients distributions

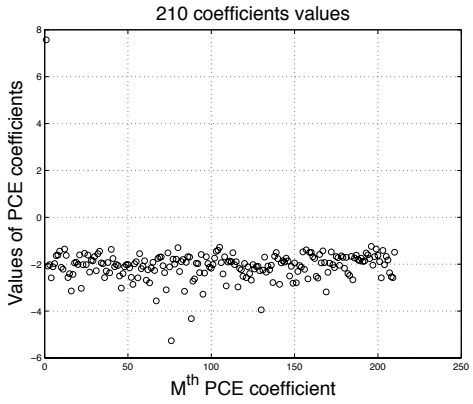

Fig. 2. PCE coefficients values

4. PCE-SKF BASED OD

In this section, the PCE method is used for propagating the augmented state (orbital state and parameter) and its associated covariance in the framework of SKF. Because the PCE theory creates an estimate of the covariance matrix, there is no need to calculate the Jacobian matrix of the non-linear orbit dynamics and use the functional form of matrix in Eq. 6-9. Moreover, even if the Gaussian assumption has been widely used in moderately nonlinear systems with good performance, it might fail in certain problems. For instance, Gaussian distribution is clearly not an ideal distribution to represent errors in uncertain, positive spring coefficients. Filters with PCE provide a feasible approach to deal with non-Gaussian uncertainties associated with the state and parameter.

In the prediction step of SKF, the covariance matrix of the augmented state shown in Eq. 5 can be estimated from the PCE process instead. Because the LSR method is used for calculating PCE coefficients, a Monte Carlo (or other

sampling methods such as Halton) samples are generated. The approximate predicted covariance can be obtained by using statistical averages of the experimental state samples (with a large number) predicted by the system dynamical model:

$$\begin{bmatrix} \hat{\boldsymbol{P}}_x & \hat{\boldsymbol{P}}_{xp} \\ \hat{\boldsymbol{P}}_{px} & \hat{\boldsymbol{P}}_p \end{bmatrix}_k^- = \frac{\left(\boldsymbol{X}_k^e - \bar{\boldsymbol{X}}_k^e\right)\left(\boldsymbol{X}_k^e - \bar{\boldsymbol{X}}_k^e\right)^T}{K} \tag{31}$$

where $\boldsymbol{X}_k^e$ (*resp.* $\bar{\boldsymbol{X}}_k^e$) denotes the experimental state sample (*resp.* the mean of the experimental state sample) from the PCE process, and K is the number of samples.

After the same process of update step of the SKF in Eq. 10-12, the covariance matrix of the state is updated with new observations. It is used as input into the PCE process in the next epoch based on the copula theory introduced in Section 3.1.

5. NUMERICAL EXAMPLES

5.1. OBSERVATION SIMULATION AND FILTERING SETTINGS

The proposed PCE-SKF algorithm is applied to orbit determination for space objects in the high altitude region (e.g. the geosynchronous orbit), where the solar radiation pressure is one of the largest non-gravitational perturbations and can therefore have significant influence on their orbital dynamics. A variety of models have been used to study solar radiation pressure for various applications. Among them, the simplest model is the cannonball model, which assumes that the force caused by solar radiation pressure acts along the object-Sun line and the object is in a cannonball-like shape with uniform optical properties in space. But it is not sufficient enough for the analysis of SRP acceleration with a constant SRP coefficient. In this study, it is assumed that the error of the SRP model is absorbed by the SRP coefficient. Our focus is to account for this type of uncertainty in the OD process. The acceleration of SRP is formulated as the following Eq. 32 for the cannonball assumptions:

$$\boldsymbol{a}_{\text{SRP}} = \frac{P_{\text{SR}} C_{\text{R}} A_{\text{S}}}{m} \boldsymbol{r}_s \tag{32}$$

where P_{SR} denotes the solar radiation pressure constant, C_{R} denotes the solar pressure parameter, A_{S} denotes the effective area facing the Sun, m is the object mass and $\boldsymbol{r}_s$ denotes the vector from the object to the Sun.

Table 1. Satellite Force Model

Satellite model	Cannon-ball model (constant surface and mass) [10]
Earth gravity field	GGM03S (20×20) [19]
Planetary ephemerides	Low precision model for the Sun, Moon, Mars, Mercury, Venus, Jupiter, Saturn, Uranus, Pluto [10]
Solar Radiation Pressure	Assumes the surface normal is always aligned with the Sun. Includes eclipses and distance from the sun. [10]
Coordinates transformations	IERS1996/IAU1980 transformations [10]

An IGSO is simulated to demonstrate the orbit determination process with force models given in Table 1. The orbital model incorporates gravitational perturbations from all planetary bodies in the solar system in addition to a high fidelity gravity model of the Earth. As for nonconservative forces, only SRP is considered with the acceleration model given in Eq. 32. The initial state of the reference orbit is given in Table 2 and satellite's parameters are given in Table 3. Three ground stations (see Table 4 for the location information) are chosen for measurements simulation. An elevation mask of 20° with an interval of 30s is used for all the measurements.

Table 2. Satellite Initial Conditions in ECI Coordinate System (m, m/s)

x (m)	y (m)	z (m)	vx (m/s)	vy (m/s)	vz (m/s)
37334419.253	6402992.005	-13817229.687	-1259.3	2409.9	-1709.8

For the filters, the orbital model is the same with that used for observation simulation, except that the SRP coefficient is set as 1.2. No process noise is considered in this study. So only the SRP modelling error due to the SRP coefficient deviation will be handled in the filter. An offset of 1m is given to each position component of the initial

Table 3. Satellite's Parameters

Satellite's mass (kg)	SPR effective area (m^2)	SPR coefficient
1800	110.5	1.0

Table 4. Ground Stations Location

ID	Location	Lattitude	Longitude
Yarragadee	WA, Australia	$-29.0464°$	$115.3467°$
Mount Stromlo	ATC, Australia	$-35.3161°$	$149.0099°$
Tanegashima	Japan	$30.5565°$	$131.0154°$

Table 5. Filters' Initial Condition in ECI Coordinate System

x (m)	y (m)	z (m)	vx (m/s)	vy (m/s)	vz (m/s)
37334420.253	6402993.005	-13817230.687	-1259.3	2409.9	-1709.8
SRP coefficient			1.2		

orbital state in comparison with the reference orbit (see Table 4). Accordingly, the initial covariance matrix for the orbital state is given by:

$$\boldsymbol{P}_0 = \text{diag}\left(1.0, \quad 1.0, \quad 1.0, \quad 1.0^{-6}, \quad 1.0^{-6}, \quad 1.0^{-6}\right)(m, m/s). \tag{33}$$

For the SRP coefficient, two distributions are used to represent its uncertainty: Gaussian and uniform distributions, with a variance value of 0.2 and an interval of $\left[1.1, \quad 1.3\right]$, respectively.

5.2. ORBIT DETERMINATION SOLUTIONS

Orbit determination solutions are generated by EKF, SKF, PCE-EKF and PCE-SKF. The position and velocity estimates in the Earth Centred Earth Fixed (ECEF) coordinate system are plotted in Fig. 3 and Fig. 4, respectively. In these simulations, 4^{th} degree of PCE is employed. The SRP coefficient is assumed as Gaussian distributed in the PCE-SKF algorithm. Due to the fact that the process noises are not added in the filter, generally the STDs (Standard Deviation) of errors are smaller than the RMS (Root Mean Square) values. As for the x component of the position, the filtering solutions with PCE fluctuate more heavily than the solutions without PCE. In other two directions, both the EKF-PCE and SKF-PCE solutions are more stable than the EKF and SKF solutions. The statistics of the state estimate is shown in Table 6 - 9. With PCE for covariance matrix propagation, the orbital state estimation could be improved significantly. For instance, the 3D RMS of the positioning errors is reduced from 0.244m by SKF to 0.121m by SKF-PCE, and the 3D RMS of the velocity estimation errors is reduced from 3.336×10^{-4}m by SKF to 2.082×10^{-4}m by SKF-PCE.

Table 6. EKF Solutions - ECEF Coordinate System

	x (m)	y (m)	z (m)	3D (m)	vx (m/s)	vy (m/s)	vz (m/s)	3D (m/s)
MEAN	-0.003	-0.054	0.040	$\sim$	2.052e-3	-1.888e-4	6.655e-6	$\sim$
STD	0.012	0.127	0.085	0.153	1.580e-4	1.673e-4	1.971e-4	3.030e-4
RMS	0.012	0.137	0.093	0.166	1.581e-4	2.513e-4	1.956e-4	3.555e-4

Table 7. PCE-EKF Solutions - ECEF Coordinate System

	x (m)	y (m)	z (m)	3D (m)	vx (m/s)	vy (m/s)	vz (m/s)	3D (m/s)
MEAN	6.381e-4	0.048	0.124	$\sim$	-4.332e-5	-8.827e-5	7.867e-5	$\sim$
STD	0.050	0.046	0.073	0.099	2.486e-5	1.069e-5	2.525e-5	3.701e-5
RMS	0.118	0.057	0.099	0.165	3.246e-5	2.520e-5	1.265e-4	1.330e-4

To evaluate the impact of the SRP coefficient in the orbit determination solutions, both Gaussian and uniform distributions are used in the PCE process to quantify the uncertainty associated with the SRP coefficient. PCE-SKF

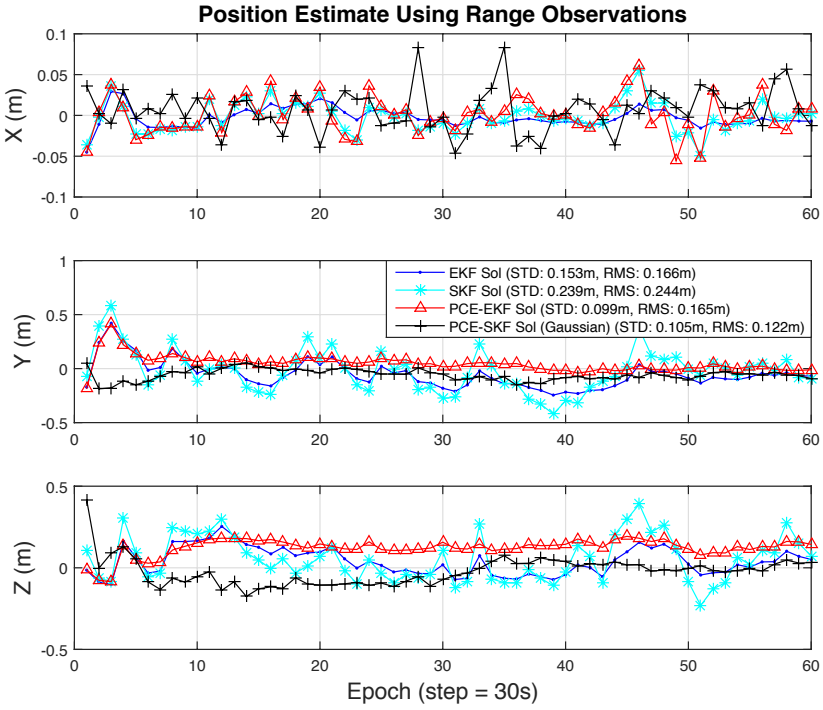

Fig. 3. Satellite Position Estimate Using Different Filters

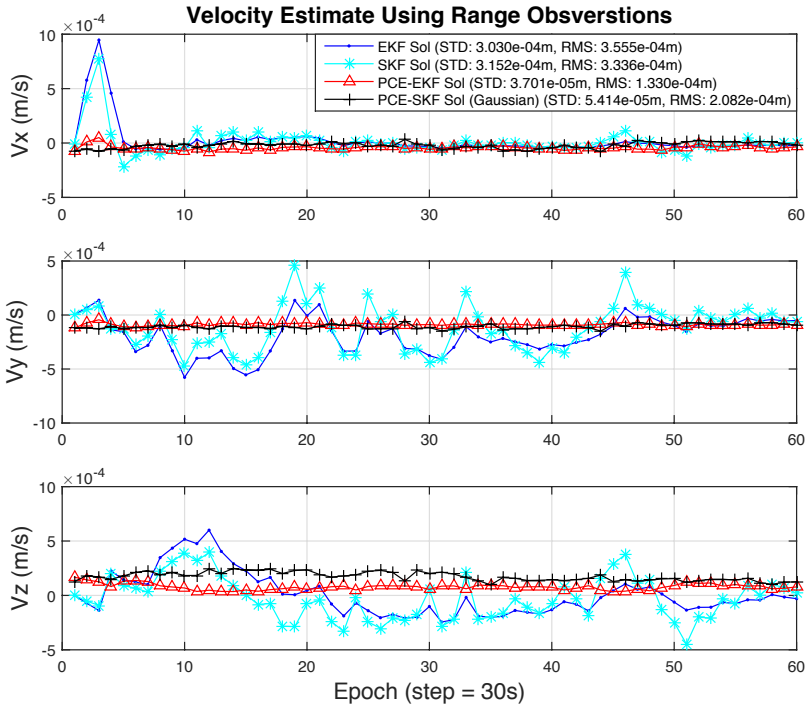

Fig. 4. Satellite Velocity Estimates Using Different Filters

Table 8. SKF Solutions - ECEF Coordinate System

	x (m)	y (m)	z (m)	3D (m)	vx (m/s)	vy (m/s)	vz (m/s)	3D (m/s)
MEAN	-0.002	-0.021	0.054	$\sim$	8.670e-6	-1.125e-3	-2.943e-5	$\sim$
STD	0.018	0.193	0.140	0.239	1.286e-4	2.099e-4	1.968e-4	3.152e-4
RMS	0.018	0.192	0.149	0.244	1.278e-4	2.366e-4	1.974e-4	3.336e-4

Table 9. PCE-SKF Solutions - ECEF Coordinate System (Gaussian Distribution for the SRP Coefficient)

	x (m)	y (m)	z (m)	3D (m)	vx (m/s)	vy (m/s)	vz (m/s)	3D (m/s)
MEAN	0.007	-0.058	-0.023	$\sim$	-2.112e-5	-1.055e-4	1.728e-4	$\sim$
STD	0.064	0.030	0.081	0.108	2.676e-5	1.589e-5	1.951e-5	3.673e-5
RMS	0.068	0.046	0.083	0.117	6.041e-5	4.996e-5	2.234e-4	2.367e-4

based satellite position estimates are plotted in Fig. 5. With the Gaussian SRP coefficient, the RMS of state estimation errors in the ECEF coordinate system is

$$[0.068, 0.046, 0.083, 6.041 \times 10^{-5}, 4.996 \times 10^{-5}, 2.234 \times 10^{-4}](m, m/s),$$

while that with the uniform SRP coefficient is

$$[0.068, 0.046, 0.083, 5.846 \times 10^{-5}, 4.948 \times 10^{-5}, 2.223 \times 10^{-4}](m, m/s).$$

Both two solutions are constrained in the 3σ threshold of the variance and they match well through the entire processing period except some slight deviations occur after the 35^{th} epoch. The 3D RMS of the state estimation errors are $[0.117, 2.367 \times 10^{-4}](m, m/s)$ with the Gaussian distributed SRP coefficient and $[0.117, 2.351 \times 10^{-4}](m, m/s)$ with the uniform distributed SRP coefficient, respectively.

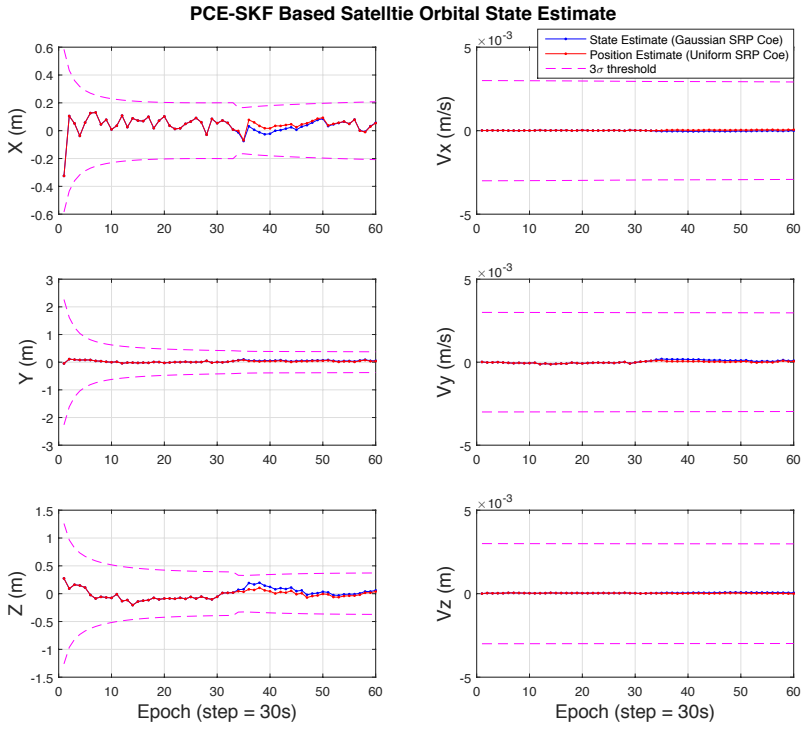

Fig. 5. Satellite Orbital State Estimate with Different SRP Coefficient Distributions Using PCE-SKF(6^{th} Degree PCE)

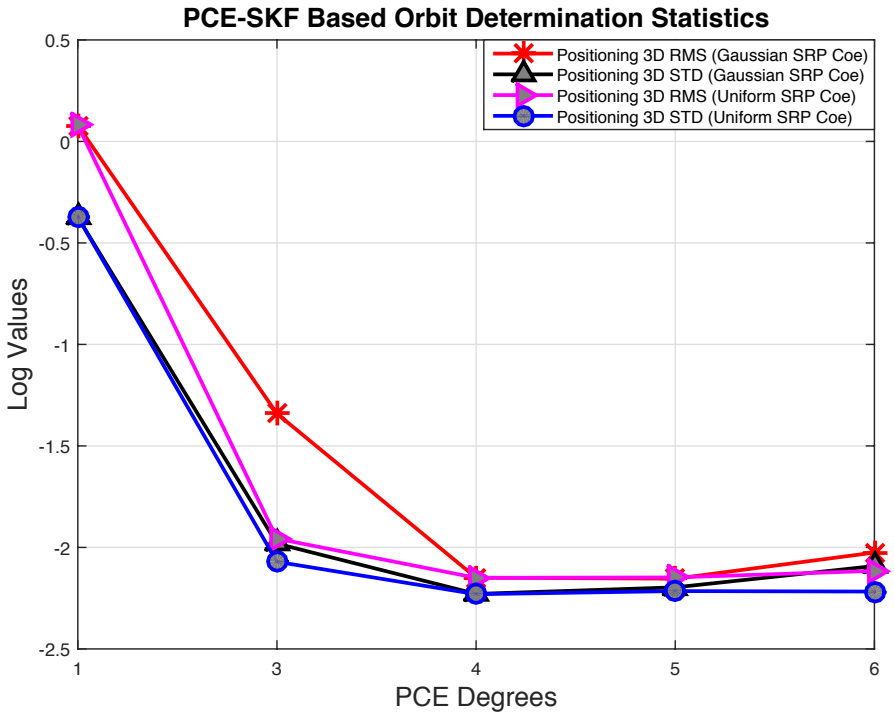

Fig. 6. PCE-SKF Based Orbit Statistics with Respect to PCE Degrees

PCE-SKF with different PCE degrees have been tested for orbit determination. The logarithmic statistic values (STD and RMS) are plotted in Fig. 6. The error statistics drops down as the degree of PCE increases. But after the 4^{th} degree, the OD errors become stable. From these statistic values, the OD solutions with a uniform distributed SRP coefficient are even somewhat better than those with a Gaussian distributed SRP coefficient.

6. CONCLUDING REMARKS

In this paper, a PCE-SKF algorithm was introduced for orbit determination of space objects, which utilises the polynomial chaos expansion for orbit state and covariance propagation in the Schmidt-Kalman filter framework with an additional orbital parameter considered. The major advantage of PCE is that it can propagate non-Gaussian uncertainties. Both Gaussian and uniform distributions were used for SRP coefficient quantification and its impact into OD accuracy was analysed. Additionally with the samples generated in PCE, the covariance propagation leads to more precise OD solutions in comparison with those based on linear propagation of covariance by STM and SM. It implies that PCE-SKF can provide more precise solutions to OD with uncertain SRP parameter handled in the simulated orbit scenario. This paper presented some preliminary OD solutions with an IGSO satellite, but it is feasible to apply the proposed PCE-SKF algorithm to other scenarios with uncertain dynamical parameters.

7. ACKNOWLEDGMENTS

The authors would like to acknowledge the support of the Cooperative Research Centre for Space Environment Management (SERC Limited) through the Australian Government's Cooperative Research Centre Programme. We also thank Dr Stefano Marelli from ETH Zürich for assistance in using UQLab software.

8. REFERENCES

1. Stanley F Schmidt. Application of state-space methods to navigation problems. *Advances in Control Systems*, 3:293–340, 1966.

2. Drew Woodbury and John Junkins. On the consider Kalman filter. In *AIAA Guidance, Navigation, and Control Conference, AIAA Paper: 2010–7752*, 2010.

3. Renato Zanetti and Chris D'Souza. Recursive implementations of the consider filter. In *Proceedings of the Jer-Nan Juang Astrodynamics Symposium, Univelt Inc., San Diego, CA*, pages 297–313, 2012.

4. Jason Stauch and Moriba Jah. Unscented schmidt-kalman filter algorithm. *Journal of Guidance, Control, and Dynamics*, 38(1):117–123, 2014.

5. Yang Yang, Xiaokui Yue, and Andrew G. Dempster. GPS-based onboard real-time orbit determination for LEO satellites using consider Kalman filter. *IEEE Transactions on Aerospace and Electronic Systems*, 52(2):769–777, April 2016.

6. Dongbin Xiu and George Em Karniadakis. The Wiener–Askey polynomial chaos for stochastic differential equations. *SIAM journal on scientific computing*, 24(2):619–644, 2002.

7. Jia Li and Dongbin Xiu. A generalized polynomial chaos based ensemble kalman filter with high accuracy. *Journal of Computational Physics*, 228(15):5454–5469, 2009.

8. Emmanuel D Blanchard, Adrian Sandu, and Corina Sandu. A polynomial chaos-based kalman filter approach for parameter estimation of mechanical systems. *Journal of Dynamic Systems, Measurement, and Control*, 132(6):061404, 2010.

9. Reza Madankan, Puneet Singla, Tarunraj Singh, and Peter D. Scott. Polynomial-chaos-based bayesian approach for state and parameter estimations. *Journal of Guidance, Control, and Dynamics*, 36(4):1058–1074, 2013.

10. Oliver Montenbruck and Eberhard Gill. *Satellite orbits: models, methods, and applications*. Springer, 2000.

11. Norbert Wiener. The homogeneous chaos. *American Journal of Mathematics*, 60(4):897–936, 1938.

12. Oliver Le Maitre and Omar M. Knio. *Spectral Methods for Uncertainty Quantification: With Applications to Computational Fluid Dynamics*. Scientific Computation. Springer Netherlands, 2010.

13. M. Munoz Zuniga, S. Kucherenko, and N. Shah. Metamodelling with independent and dependent inputs. *Computer Physics Communications*, 184(6):1570–1580, 2013.

14. Marc Berveiller, Bruno Sudret, and Maurice Lemaire. Stochastic finite element: a non intrusive approach by regression. *European Journal of Computational Mechanics*, 15(1–3):81–92, 2006.

15. Sudret Bruno. *Polynomial chaos expansions and stochastic finite-element methods*, book section 6, pages 265–300. CRC Press, 2014. doi:10.1201/b17970-9.

16. Roger B Nelsen. *An introduction to copulas*. Springer Science & Business Media, 2007.

17. Régis Lebrun and Anne Dutfoy. A generalization of the nataf transformation to distributions with elliptical copula. *Probabilistic Engineering Mechanics*, 24(2):172–178, 2009.

18. MS Eldred and John Burkardt. Comparison of non-intrusive polynomial chaos and stochastic collocation methods for uncertainty quantification. In *Proceedings of the 47th AIAA aerospace science meeting and exhibit, AIAA-2009-0976*, pages 1–20, 2009.

19. B Tapley, J Ries, S Bettadpur, D Chambers, M Cheng, F Condi, and S Poole. The GGM03 mean earth gravity model from GRACE. In *AGU Fall Meeting Abstracts*, volume 1, page 03, 2007.